

Nonlocal PNJL model beyond mean field and the QCD phase transition

A.E. Radzhabov,^{1,*} D. Blaschke,^{2,3,†} M. Buballa,^{4,‡} and M.K. Volkov^{3,§}

¹*Institute for System Dynamics and Control Theory, 664033 Irkutsk, Russia*

²*Institute for Theoretical Physics, University of Wrocław, 50-204 Wrocław, Poland*

³*Bogoliubov Laboratory of Theoretical Physics, JINR Dubna, 141980 Dubna, Russia*

⁴*Institut für Kernphysik, Technische Universität Darmstadt, D-64289 Darmstadt, Germany*

A nonlocal chiral quark model is consistently extended beyond mean field using a strict $1/N_c$ expansion scheme. The parameters of the nonlocal model are refitted so that the physical values of the pion mass and the weak pion decay constant are obtained. The size of the $1/N_c$ correction to the quark condensate is carefully studied and compared with the usual local Nambu–Jona-Lasinio model. It is found that even the sign of the corrections can be different. This can be attributed to the mesonic cut-off of the local model. The model is also applied to finite temperature. We find that the $1/N_c$ corrections dominate the melting of the chiral condensate at low temperatures, $T \lesssim 100$ MeV, in agreement with chiral perturbation theory. On the other hand, the relative importance of the $1/N_c$ corrections in the cross-over regime depends on the parameter T_0 of the Polyakov loop potential. For $T_0 = 270$ MeV, corresponding to a fit of lattice data for pure gluodynamics, the correction terms are large and lead to a lowering of the chiral phase transition temperature in comparison with the mean-field result. Near the phase transition the $1/N_c$ expansion breaks down and a non-perturbative scheme is needed to include mesonic correlations in that regime. Lowering T_0 leads to a more rapid cross-over even at the mean-field level and the unstable region for the $1/N_c$ corrections shrinks. For $T_0 \lesssim 220$ MeV the temperatures of deconfinement and chiral restoration are practically synchronized.

PACS numbers: 11.10.Wx, 12.38.Aw, 12.38.Mh, 12.39.Fe

I. INTRODUCTION

A quantum field theoretical description of strong interactions in the nonperturbative regime is one of the most interesting and challenging problems of present-day theoretical physics. Quantum chromodynamics is well known only at the perturbative level whereas the low-energy region and the most interesting “hadronic” phase in the QCD phase diagram is in the nonperturbative regime. The only nonperturbative *ab initio* calculations are performed in lattice QCD, but their range of applicability is still limited. To gain some analytical insights to non-perturbative QCD, continuum approaches, even using effective models, are legitimate tools. They may provide a theoretical interpretation of results from lattice QCD and allow their extrapolation to otherwise inaccessible domains.

One of the successful models for a description of chiral quark dynamics and the phase diagram is the Nambu–Jona-Lasinio (NJL) model [1] applied to quarks [2–5]. This model provides a mechanism for spontaneous chiral symmetry breaking and the formation of a quark condensate. The low-lying hadron spectrum, low-energy dynamics, the main strong and electromagnetic decays, hadron-hadron scattering and the internal characteristics of mesons have a reasonable explanation within this

model. A generalization of the NJL model has been proposed which includes the coupling of the chiral quark sector to the Polyakov loop, being an order parameter of the deconfinement transition (PNJL model [6–15]). The temperature dependent parameters of the effective Polyakov loop potential are fitted by using lattice QCD data on pure gluodynamics.

Nonlocal generalizations of the PNJL model provide an approach to the 4-momentum dependence of the quark mass function and wave function renormalization of the quark propagator [13–17], thus allowing to implement detailed nonperturbative information about low-energy QCD dynamics accessible, e.g., in *ab-initio* LQCD simulations [18–20]. Recently, a justification of nonlocal PNJL models as effective low-energy limit of QCD has been given [17], based in part on methods of the Wilsonian renormalization group [21].

Usually, NJL and PNJL models are formulated at the mean-field level. However, there are physical problems where the mean-field formulation is not sufficient. Large corrections to the mean-field behavior can be expected, e.g., in the description of broad resonances from their coupling to intermediate meson states¹ and for the equation of state of the hadronic phase where quark and gluon degrees of freedom are “frozen” in condensates and hadronic bound states are carrying all dynamics and thus represent the physical degrees of freedom.

*Electronic address: aradzh@icc.ru

†Electronic address: blaschke@ift.uni.wroc.pl

‡Electronic address: michael.buballa@physik.tu-darmstadt.de

§Electronic address: volkov@theor.jinr.ru

¹ The σ -meson with a decay width of the order of its mass is the most striking example of such state. See, e.g., “Note on scalar mesons” in [22].

There are different schemes to go beyond the mean-field level [23–33]. One of the most promising ones is based on a strict expansion of the inverse number of quark colors, $1/N_c$, which is a natural expansion parameter for gauge theories [34]. The local NJL model is non-renormalizable and therefore it is necessary to introduce an additional cut-off parameter when going beyond the mean-field level. This problem is absent in nonlocal versions of the NJL model where the nonlocality leads to an effective regularization which renders the quark (multi)-loop diagrams convergent.

In the present paper the $SU(2) \times SU(2)$ nonlocal PNJL model is investigated beyond mean field within a strict $1/N_c$ expansion scheme at finite temperature and zero chemical potential. This study aims to quantify the effect of mesonic excitations on the chiral restoration temperature and to demonstrate that the behavior of the chiral condensate at low-temperatures is in accordance with the exact results of chiral perturbation theory. We also investigate the dependence of the results on the parameter T_0 of the Polyakov-loop potential.

II. NONLOCAL MODEL IN VACUUM

We begin with the discussion of our nonlocal model in vacuum. The main goal is to fix the model parameters by calculating meson properties at next-to-leading order in $1/N_c$. It is well-known that in the local PNJL model at $T = 0$ the gluon sector decouples from the quark sector, so that the latter is reduced to the standard NJL model. The same is true in the nonlocal model. In this section we can therefore restrict ourselves to the quark sector, while the Polyakov-loop dynamic will be introduced in Sec. III.

A. Mean field

The quark sector of the nonlocal chiral quark model is described by the Lagrangian

$$\mathcal{L}_q = \bar{q}(x)(i\cancel{\partial} - m_c)q(x) + \frac{G}{2}[J_\sigma^2(x) + \vec{J}_\pi^2(x)], \quad (1)$$

where m_c is the current quark mass. The nonlocal quark currents are

$$J_M(x) = \int d^4x_1 d^4x_2 f(x_1)f(x_2) \times \bar{q}(x - x_1)\mathbf{\Gamma}_M q(x + x_2), \quad (2)$$

where $\mathbf{\Gamma}_\sigma = 1$, $\mathbf{\Gamma}_\pi = i\gamma^5\tau^a$ with $a = 1, 2, 3$, and $f(x)$ is a form factor. The latter is defined by its Fourier transform in Euclidean space², which we take to be Gaussian,

$f^2(p_E^2) = \exp(-p_E^2/\Lambda^2)$. This scheme introducing non-local currents which we utilize throughout this work has been denoted as “instanton liquid model” as opposed to the “one-gluon exchange model” scheme, see Ref. [35] for details.

After linearization of the four-fermion vertices by introducing auxiliary scalar ($\tilde{\sigma}$) and pseudoscalar (π^a) meson fields the quark sector is described by the Lagrangian³

$$\begin{aligned} \mathcal{L}_{q\pi\sigma} = & \bar{q}(x)(i\cancel{\partial} - m_c)q(x) - \frac{\pi_a^2(x) + \tilde{\sigma}^2(x)}{2G} + \\ & + J_\sigma(x)\tilde{\sigma}(x) + \pi^a(x)J_\pi^a(x). \end{aligned} \quad (3)$$

To proceed, we single out the nonzero mean-field value of the scalar field by the decomposition $\tilde{\sigma} = \sigma + \sigma_{\text{MF}}$ so that π^a and σ denote only the fluctuating parts of the fields ($\langle\pi^a\rangle = \langle\sigma\rangle = 0$) describing mesonic correlations. The scalar mean field gives a dynamical contribution to the quark mass, i.e., the dressed quark propagator becomes

$$S(p) = (\cancel{p} - m(p^2))^{-1} = (\cancel{p} - m_c - \Sigma(p))^{-1}, \quad (4)$$

with the quark self-energy

$$\begin{aligned} \Sigma(p) = & iG\Gamma^\sigma(p, p) \int \frac{d^4k}{(2\pi)^4} \text{Tr} [\Gamma^\sigma(k, k) S(k)] \\ \equiv & m_d f^2(p^2). \end{aligned} \quad (5)$$

Here the symbol Tr stands for the trace over color-, flavor- and Dirac-indices, and $\mathbf{\Gamma}^M(q_1, q_2) = \mathbf{\Gamma}_M f(q_1^2)f(q_2^2)$ is the nonlocal generalization of the meson-quark-antiquark vertex function with the quark and antiquark momenta q_1 and q_2 , respectively. In the following, we will often use a shorthand subscript notation for the momentum dependence of functions, e.g., $f_k \equiv f(k^2)$ and $\Gamma^\sigma(q_1, q_2) \equiv \Gamma_{q_1, q_2}^\sigma$.

The amplitude $m_d = -\sigma_{\text{MF}}$ is an order parameter for dynamical chiral symmetry breaking. The chiral condensate per flavor,

$$\langle\bar{q}q\rangle^{\text{MF}} = -\frac{i}{2} \int \frac{d^4k}{(2\pi)^4} \text{Tr} [S^{np}(k)], \quad (6)$$

is obtained from the non-perturbative part of the quark propagator, $S^{np}(p) = S(p) - S^c(p)$, i.e., after subtracting the perturbative part $S^c(p) = (\cancel{p} - m_c)^{-1}$.

Mesons are described as bound state solutions of the quark-antiquark Bethe-Salpeter equation. The meson propagators are given by

$$D_p^M = \frac{1}{-G^{-1} + \Pi_p^M}, \quad (7)$$

where $M = \pi, \sigma$ and $\Pi_p^M \equiv \Pi_M^{\text{MF}}(p^2)$ are the mean field polarization functions defined by

$$\Pi_p^M = i \int \frac{d^4k}{(2\pi)^4} \text{Tr} [S_{k_-} \Gamma_{k_-, k_+}^M S_{k_+} \Gamma_{k_+, k_-}^M], \quad (8)$$

² Unless stated otherwise, the expressions in this paper are given in Minkowski space. The transformation to Euclidean space is trivial for energies below the (pseudo)threshold (see Sect. II C).

³ Note, that after bosonization the possible exchange (Fock) terms between quark currents are eliminated.

where $k_{\pm} = k \pm p/2$.

The meson masses are the poles of the propagators at $p^2 = (M_M^{\text{MF}})^2$ obtained by solving

$$-G^{-1} + \Pi_M^{\text{MF}}((M_M^{\text{MF}})^2) = 0. \quad (9)$$

Let us consider the pion case. In the vicinity of the pole the pion propagator can be expanded as

$$D_p^{\pi} \simeq \frac{(g_{\pi}^{\text{MF}})^2}{p^2 - (M_{\pi}^{\text{MF}})^2} + \text{regular terms}, \quad (10)$$

where g_{π}^{MF} is the pion-quark-antiquark coupling constant

$$(g_{\pi}^{\text{MF}})^{-2} = \left. \frac{\partial \Pi_{\pi}^{\text{MF}}(p^2)}{\partial p^2} \right|_{p^2=(M_{\pi}^{\text{MF}})^2} \quad (11)$$

To calculate the weak pion decay constant, the pion solutions of the Bethe-Salpeter equation have to be coupled to an external weak current. To that end the Lagrangian (3) must be modified so that it becomes invariant under local vector and axial-vector gauge transformations. In nonlocal models this is complicated by the fact that not only the kinetic part but also the interaction is not gauge invariant by itself, so that in addition to the usual covariant derivative one has to take into account the coupling of the external fields to the nonlocal quark vertices. This can be done by delocalization of the quark fields [35–40]

$$q(y) \rightarrow Q(x, y) = E(x, y)q(y) \quad (12)$$

where

$$E(x, y) = \mathcal{P} \exp \left\{ i \int_x^y dz^{\mu} [\mathcal{V}_{\mu}^a(z) + \mathcal{A}_{\mu}^a(z) \gamma_5] T^a \right\} \quad (13)$$

is the Schwinger phase factor, involving the external vector and axial-vector gauge fields \mathcal{V}_{μ}^a and \mathcal{A}_{μ}^a , and $T^a \equiv \tau^a/2$. For the kinetic part it can be shown that this replacement is equivalent to minimal substitution, hence leading to the standard electroweak vertices. In the interaction Lagrangian, on the other hand, the nonlocal quark currents Eq. (2) are replaced by

$$J_M(x) = \int d^4x_1 d^4x_2 f(x_1) f(x_2) \times \\ \times \bar{Q}(x - x_1, x) \Gamma_M Q(x, x + x_2), \quad (14)$$

giving rise to additional vertex contributions. One of them is related to the coupling of J_{σ} to the scalar mean-field σ_{MF} and contributes, together with the bare vertex extracted from the kinetic part, to the vertex function depicted on the left of Fig. 1. The other contributions originate from J_M coupled to the fluctuating meson fields and lead to the vertex functions shown on the right of Fig. 1.

Although the above procedure is sufficient to ensure gauge invariance, in general it does not unambiguously fix

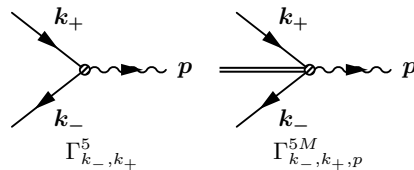


FIG. 1: Vertices of weak currents (wavy lines) coupled to a quark (left) and to the non-local quark-meson vertices (right).

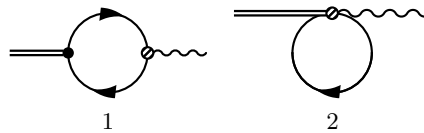


FIG. 2: Weak pion decay at mean field.

the vertex structure. To this end, it is necessary to define rules for the evaluation of the line integral in Eq. (13). This can be done by specifying the integration path, e.g., as a straight line [35, 37, 38, 40], or by making use of the path independent definition of the derivative of the line integral [36, 39]. However, for the pion decay constant we only need the longitudinal projection of the vertices, which are related to axial Ward-Takahashi identities and therefore do not depend on the integration path. The results read

$$\Gamma_{k_-, k_+}^{5, L} = -\frac{1}{p^2} \left(S_{k_-}^{-1} \gamma_5 T^a + \gamma_5 T^a S_{k_+}^{-1} + \right. \\ \left. + 2(m_c + m_d f_{k_-} f_{k_+}) \gamma_5 T^a \right), \\ \Gamma_{k_-, k_+}^{5M, L} = -\frac{1}{p^2} \left[(f_{k_+} - f_{k_+ - p}) f_{k_-} \gamma_5 T^a \Gamma_M + \right. \\ \left. + (f_{k_-} - f_{k_- + p}) f_{k_+} \Gamma_M \gamma_5 T^a \right]. \quad (15)$$

Accordingly, the pion decay constant at the mean-field level contains two pieces, $f_{\pi}^{\text{MF}}(p^2) = f_{\pi, 1}^{\text{MF}}(p^2) + f_{\pi, 2}^{\text{MF}}(p^2)$, which are displayed in Fig. 2. Evaluating these diagrams one finds

$$f_{\pi, 1}^{\text{MF}}(p^2) = g_{\pi}^{\text{MF}} \int \frac{d^4k}{(2\pi)^4} \text{Tr} \left[\Gamma_{k_+, k_-}^{\pi} S_{k_-} \Gamma_{k_-, k_+}^{5, L} S_{k_+} \right] \\ f_{\pi, 2}^{\text{MF}}(p^2) = g_{\pi}^{\text{MF}} \int \frac{d^4k}{(2\pi)^4} \text{Tr} \left[\Gamma_{k, k}^{5\pi, L} S_k \right], \quad (16)$$

With the definition of the pion mass and weak decay constant two of the three parameters (m_c , Λ , $G\Lambda^2$) of the nonlocal model can be fixed with the vacuum values of these observables.

B. $1/N_c$ corrections beyond mean field

As usual in the systematic $1/N_c$ expansion, the four-quark coupling constant G is considered to be of the order

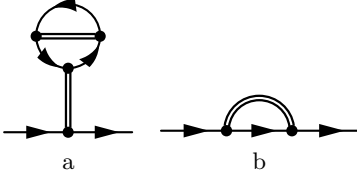


FIG. 3: $1/N_c$ corrections to the quark selfenergy.

$1/N_c$. In this case the N_c behavior of pion properties calculated in the model coincides with leading-order QCD calculations ($f_\pi \sim \sqrt{N_c}$). As a result any meson propagator line in diagrams has a $1/N_c$ suppression factor.

The next-to-leading $1/N_c$ correction Σ^{N_c} to the quark selfenergy corresponds to the diagrams displayed in Fig. 3 [27–29]. From these diagrams one obtains

$$\Sigma_p^{N_c} = C f_p^2 - \sum_{M=\sigma,\pi} i \int \frac{d^4 l}{(2\pi)^4} [D_l^M \Gamma_{p,p-l}^M S_{p-l} \Gamma_{p-l,p}^M],$$

where

$$C = D_0^\sigma \zeta, \quad \zeta = \sum_{M=\sigma,\pi} i \int \frac{d^4 l}{(2\pi)^4} D_l^M \Gamma_{l,l}^{\sigma MM}, \quad (17)$$

and $\Gamma_{q_1, q_2}^{\alpha\beta\gamma}$ is the quark triangle diagram for the three-meson vertex. For external mesons α , β and γ the quark triangle has the following form

$$\Gamma_{q_1, q_2}^{\alpha\beta\gamma} = -i \int \frac{d^4 k}{(2\pi)^4} \text{Tr} \times \left[\Gamma_{k+q_1, k+q_2}^\alpha S_{k+q_2} \Gamma_{k+q_2, k}^\beta S_k \Gamma_{k, k+q_1}^\gamma S_{k+q_1} \right]. \quad (18)$$

When $q_1 = q_2 = l$, the three-meson vertices in Euclidean space are

$$\Gamma_{l,l}^{\sigma MM} = -4N_c N_f \int \frac{d^4_E k}{(2\pi)^4} \frac{f_k^2 f_{k+l}^4}{D_k D_{k+l}^2} \times \left[2k \cdot (k+l) m_{k+l} \pm m_k ((k+l)^2 + m_{k+l}^2) \right], \quad (19)$$

where the upper sign corresponds to $M = \sigma$, the lower sign to $M = \pi$ and $D_k = k^2 + m_k^2$ is the denominator of the quark propagator.

From the $1/N_c$ corrections to the quark selfenergy it follows for the quark propagator

$$S_p^{\text{MF}+N_c} = (S_p^{-1} - \Sigma_p^{N_c})^{-1} = S_p + S_p \Sigma_p^{N_c} S_p + \text{higher orders}, \quad (20)$$

which, in turn, gives rise to $1/N_c$ corrections to the quark condensate (cf. Eq. (6)). According to the two selfenergy corrections shown in Fig. 3, there are two contributions, $\langle \bar{q}q \rangle^{N_c} = \langle \bar{q}q \rangle^{N_c, a} + \langle \bar{q}q \rangle^{N_c, b}$, which are given by

$$\langle \bar{q}q \rangle^{N_c, a} = -C \Pi_0^{\sigma, a}, \quad \langle \bar{q}q \rangle^{N_c, b} = \zeta^b, \quad (21)$$

where $\Pi_p^{\sigma, a}$ can be obtained from Eq. (8) for Π_p^σ by substituting the form factors in the numerator of the function $f_{k_+}^2 f_{k_-}^2 \rightarrow$

$f_{k_+} f_{k_-}$ and ζ^b can be obtained from ζ by substituting the form factors in the numerator of the function $\Gamma_{l,l}^{\sigma MM}$, Eq. (19), $f_{k+l}^4 \rightarrow f_{k+l}^2$.

The full pion propagator consists of a mean-field part plus $1/N_c$ corrections (details are given in the appendix)

$$\Pi_\pi^{\text{Full}}(p^2) = \Pi_\pi^{\text{MF}}(p^2) + \Pi_\pi^{N_c}(p^2) \quad (22)$$

and the pion mass can be found by solving the equation

$$-G^{-1} + \Pi_\pi^{\text{Full}}((M_\pi^{\text{Full}})^2) = 0. \quad (23)$$

The quark-meson coupling constant should be divided into mean-field part and a $1/N_c$ correction. This separation is unique only for the pion in the chiral limit. At finite m_c there are different possibilities to take into account higher order p^2 terms. In the present work we use

$$(g_\pi^{\text{Full}})^{-2} = \left. \frac{\partial \Pi_\pi^{\text{Full}}(p^2)}{\partial p^2} \right|_{p^2=(M_\pi^{\text{Full}})^2}, \quad (g_\pi^{\text{MF}})^{-2} = \left. \frac{\partial \Pi_\pi^{\text{MF}}(p^2)}{\partial p^2} \right|_{p^2=(M_\pi^{\text{MF}})^2}. \quad (24)$$

There are two sources of $1/N_c$ corrections for the weak pion decay constant. One is the correction of the meson-quark coupling constant and can be obtained from the mean-field expression, Eq. (16), by the substitution $g_\pi^{\text{MF}} \rightarrow g_\pi^{N_c} = g_\pi^{\text{Full}} - g_\pi^{\text{MF}}$. The other correction is due to new diagrams appearing at order $1/N_c$. We present details of the calculation of this correction in the appendix.

C. Vacuum results

The $1/N_c$ corrections to meson properties will affect the results for the quark condensate via the readjustment of the model parameters (Λ , m_c , $G\Lambda^2$) which are to be chosen such that the physical values for the pion mass $M_{\pi^\pm} = 139.57$ MeV and the weak pion decay constant $f_\pi = 92.42$ MeV are obtained at $T = 0$, while the dimensionless coupling $G\Lambda^2$ is left as a free parameter. Different parameterizations of the nonlocal model beyond mean field are given in Table I. The corresponding behavior of the quark condensate as a function of the dimensionless coupling is presented in Fig. 4.

One important check of the calculations is the proof of the Goldstone nature of the pion. In the case of exact chiral symmetry the pion should be massless. This check is shown in Fig. 5 where M_π^{Full} and M_π^{MF} are displayed as functions of the current quark mass for Λ and G taken from parameter set 4.

The mean-field contributions to the pion mass and weak decay constant are also listed in Table I for the different parameter sets. The corresponding $1/N_c$ corrections are shown in Fig. 6. For lower values of $G\Lambda^2$ these corrections amount to -15 MeV for the pion mass and to 20 MeV for f_π . For parameter set 4 the corrections are only about -2 MeV and 5 MeV, respectively.

TABLE I: Different parameterizations: model parameters ($\Lambda, G\Lambda^2, m_c$), the dynamical mass m_d , position of the first two poles and the corresponding (pseudo-) threshold of the mean-field quark propagator, mean-field values of the pion mass and the weak decay constant, and critical temperatures for chiral restoration and deconfinement for two values of the parameter T_0 of Polyakov loop potential. The set with the highest threshold value is highlighted. The pseudo-threshold values are shown in italics.

No.	$G\Lambda^2$	Λ	m_c	m_d	first two poles	(pseudo)threshold	M_π^{MF}	f_π^{MF}	$T_0 = 270$ MeV			$T_0 = 208$ MeV		
									T_c	T_c^{MF}	T_d	T_c	T_c^{MF}	T_d
units		MeV	MeV	MeV	GeV^2	MeV	MeV	MeV	MeV			MeV		
1	13.35	1479.2	2.82	139.2	-0.0205, -6.331	286.7, 5032.3	155.5	71.5	191	205	213	164	162	162
2	14.89	934.8	5.58	211.2	-0.0529, -1.545	459.8, 2486.0	144.6	83.4	193	206	214	166	165	166
3	17.06	705.9	8.64	269.1	-0.1262, -0.447	710.6, 1337.2	142.4	87.1	193	207	214	168	167	168
4	17.64	670.3	9.38	281.9	$-0.2291 \pm i0$	957.3	142.2	87.6	194	207	214	169	168	169
5	19.72	580.5	11.78	322.5	$-0.1082 \pm i0.1763$	<i>793.7</i>	141.7	88.7	197	208	213	170	169	170
6	22.83	500.8	14.95	373.8	$-0.0289 \pm i0.1832$	<i>654.7</i>	141.4	89.5	200	208	213	170	170	170
7	26.33	445.3	18.15	424.0	$+0.0117 \pm i0.1692$	<i>562.0</i>	141.2	90.0	202	208	212	171	171	171
8	30.20	404.4	21.37	473.4	$+0.0344 \pm i0.1536$	<i>496.0</i>	141.2	90.3	203	208	211	172	171	172

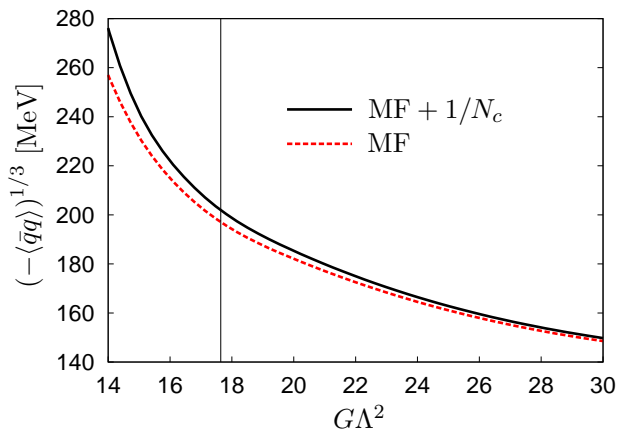


FIG. 4: (Color online) The quark condensate as a function of the dimensionless coupling $G\Lambda^2$. The result of the full $1/N_c$ corrected approach (black solid line) is compared to the mean field contribution (red dashed line). The vertical line corresponds to the parameter set No. 4.

The region of applicability of the model is closely related to the pole structure of the mean-field quark propagator and depends on the parameters. For large values of Λ , the propagator has two poles on the real p^2 axis, whereas when Λ is decreased these poles eventually merge and then go over into a pair of complex conjugate poles. (In both cases, there is an infinite number of additional complex conjugate poles, which, however, only play a minor role.) If the propagator has real poles, there is a real threshold in quark loop diagrams, i.e., for external momenta $p > p_{\text{threshold}}$ the loops have imaginary parts. The complex conjugate poles, on the other hand, lead to a so-called pseudo-threshold. In the absence of real poles the quark loops are then purely real but have a cusp at the pseudothreshold. Usually, the absence of poles on the real p^2 axis is considered as a possible criterion for quark confinement [41]. However, due to the cusp in the

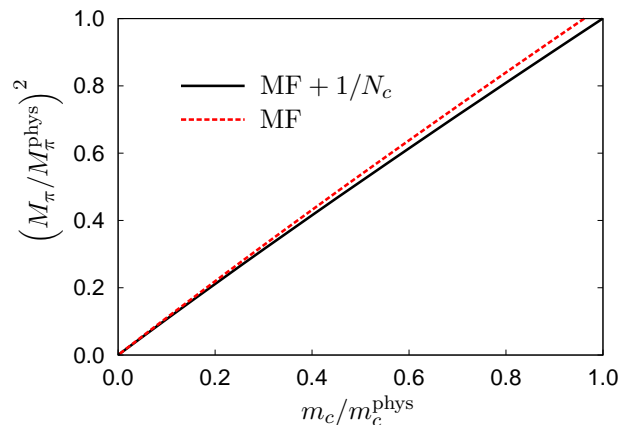


FIG. 5: (Color online) Squared pion mass normalized to the physical value versus normalized current quark mass in mean-field approximation (red dashed line) and the full $1/N_c$ corrected approach (black solid line). The values of Λ and G correspond to parameter set No. 4.

real part of the quark loop diagrams the applicability of the model above the pseudo-threshold is at least questionable.

The positions of the two lowest quark poles and the corresponding (pseudo-) thresholds of the polarization quark loop are listed in the table. The (pseudo-) thresholds are also shown in Fig. 7. There one can see that parameter set 4 corresponds to the maximal threshold value. For this reason we will use parameter set 4 in the finite T calculations in Sec. III.

D. Sign of the $1/N_c$ corrections

Our results for the $1/N_c$ -corrections to the quark condensate and to the pion decay constant are quite surprising. Naively, one would expect that taking into account

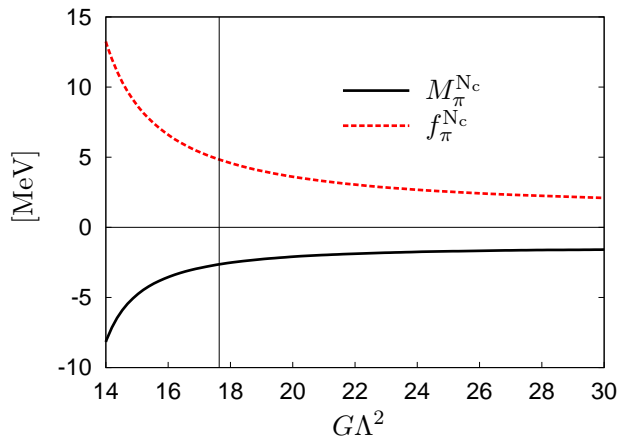


FIG. 6: (Color online) $1/N_c$ corrections to the pion mass (black solid line) and the weak pion decay constant (red dashed line).

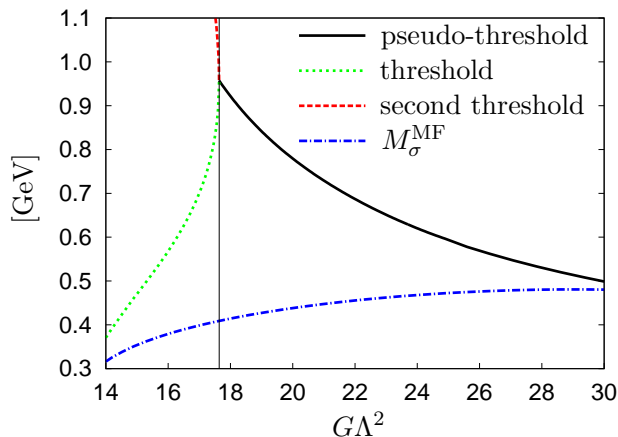


FIG. 7: (Color online) The $\bar{q}q$ -(pseudo)threshold due to the lowest singularities of quark propagator. Below a critical value of $G\Lambda^2$ (thin solid line) there are real thresholds in quark loop diagrams (green dotted line for the first singularity and red dashed line for the second one). Above this critical value the lowest singularities of the quark propagator are complex-conjugated values and there is no imaginary part of the quark loops. However, quark loops contain a pseudo-threshold (thick solid line). The blue dash-dotted line indicates the σ -meson mass at the mean field level.

meson loops should reduce the strength of spontaneous chiral symmetry breaking and, thus, reduce the values of $|\langle\bar{q}q\rangle|$ and f_π . Indeed, this is what has been found in Refs. [28, 29] for the local NJL model. However, as seen in Figs. 4 and 6, in the nonlocal model we find exactly the opposite behavior for all sets of model parameters. Obviously, this difference between the local and the nonlocal model calls for some clarification.

As pointed out before, in the nonlocal model, after introducing the Gaussian form factor, all diagrams at any order are automatically finite. This is different from the local NJL model where, because of its non-renormalizability, it is necessary to introduce indepen-

dent cutoff parameters for pure quark loops and for meson-quark loops, respectively. In [28, 29] a Pauli-Villars regularization has been used for quark loops and a three-momentum cutoff Λ_M for meson-quark loops. In order to study the transition from the nonlocal model to the local one let us construct a nonlocal model with three parameters

1. parameter of nonlocality Λ
2. parameter of quark loop regularization Λ_q
3. parameter of meson loop regularization Λ_M

The local model corresponds to the limit

$$\Lambda \rightarrow \infty, \quad \Lambda_q = \Lambda_q^{\text{fit}}, \quad \Lambda_M = \Lambda_M^{\text{fit}}, \quad (25)$$

while the nonlocal model without regularization can be obtained by setting

$$\Lambda = \Lambda^{\text{fit}}, \quad \Lambda_q \rightarrow \infty, \quad \Lambda_M \rightarrow \infty. \quad (26)$$

For definiteness, let us compare the local model [28, 29] with the nonlocal one from [13] with parameterizations fixed in the mean-field approximation. Note that for the given parameterizations, the MF quark condensates in the local and the nonlocal models agree within less than 0.5 %.

The next step is to consider the $1/N_c$ corrections and to investigate the role of the mesonic three-momentum cut-off Λ_M . For this purpose it is very instructive to study the ratio of the full quark condensate to the MF contribution $\langle\bar{q}q\rangle/\langle\bar{q}q\rangle^{\text{MF}}$. In Fig. 8 we compare the Λ_M dependence of this ratio for the local NJL model as given in Ref. [28] (dash-dotted line) to that of the nonlocal model (bold solid line) and its local limit (dashed line).⁴ It is very interesting that in the region below ~ 1.5 GeV these models predict a negative sign for the $1/N_c$ correction whereas for large mesonic cut-off the sign is positive. However, in the nonlocal model the absolute value of the correction saturates for Λ_M larger than ~ 2.5 GeV, which is well above actual parameterizations for Λ_q and Λ_M in Ref. [29]. In fact, in Ref. [28] it was found that already for $\Lambda_M \approx 1250$ MeV, the pion propagator gets unphysical poles, which was interpreted as a breakdown of the expansion. In our present model no such unphysical effects are observed.

In order to study the dependence of the sign of the $1/N_c$ correction to the quark condensate on the form factor we consider the Lorentzian-type form factor $f(p_E^2) = 1/(1 + (p_E^2/\Lambda^2)^n)$ with $n=2,5$ or 10 , see also [35, 42]. We

⁴ Note that in Ref. [28] the total quark condensate was calculated including the perturbative part, whereas in the nonlocal model and its local limit we have only considered the nonperturbative part. However, for the local model the difference for nonstrange condensate is small.

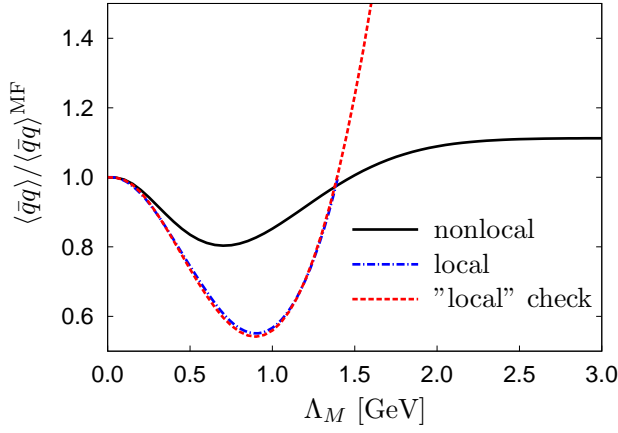


FIG. 8: (Color online) The ratio $\langle \bar{q}q \rangle / \langle \bar{q}q \rangle^{\text{MF}}$ as a function of the meson cutoff Λ_M . The full nonlocal result is shown by the black solid line. The local result (blue dash-dotted line) is taken from Fig. 3a of Ref. [28]. The "local" check (red dashed line) is the local limit of the nonlocal calculations, see Eq. (25).

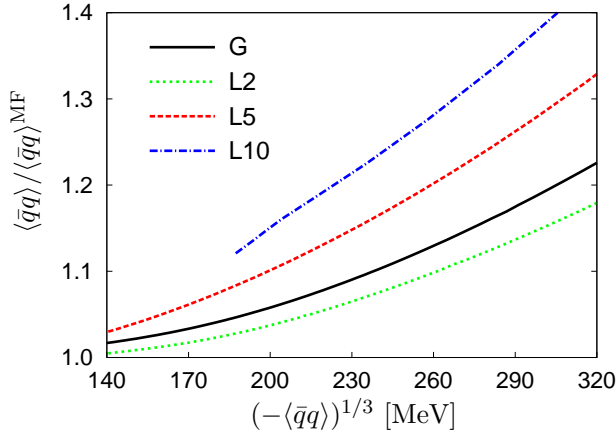


FIG. 9: (Color online) The ratio $\langle \bar{q}q \rangle / \langle \bar{q}q \rangle^{\text{MF}}$ as a function of the quark condensate for different form factors: Gaussian (G) and Lorentzian-type (L2, L5, L10) with $n=2, 5, 10$. For details, see text.

found that the sign of the $1/N_c$ correction is positive for all possible parameterizations. This is shown in Fig. 9.

A related question concerns the $1/N_c$ corrections to the quark dressing functions $A(p^2)$ and $B(p^2)$, defined by

$$S_p^{-1} = A(p^2)\not{p} - B(p^2), \quad (27)$$

or, equivalently, to the wave-function renormalization function $Z(p^2) = 1/A(p^2)$ and the mass function $M(p^2) = B(p^2)/A(p^2)$. In mean-field approximation, we have $A^{\text{MF}}(p^2) \equiv 1$ and $B^{\text{MF}}(p^2) = m_c + m_d f^2(p^2)$, see Eqs. (4) and (5). Including $1/N_c$ corrections we find that the vector dressing function $A(p^2)$ becomes enhanced, corresponding to a reduction of $Z(p^2)$. However, the scalar dressing function $B(p^2)$ increases even stronger, so that the mass function $M(p^2)$ is enhanced as well.

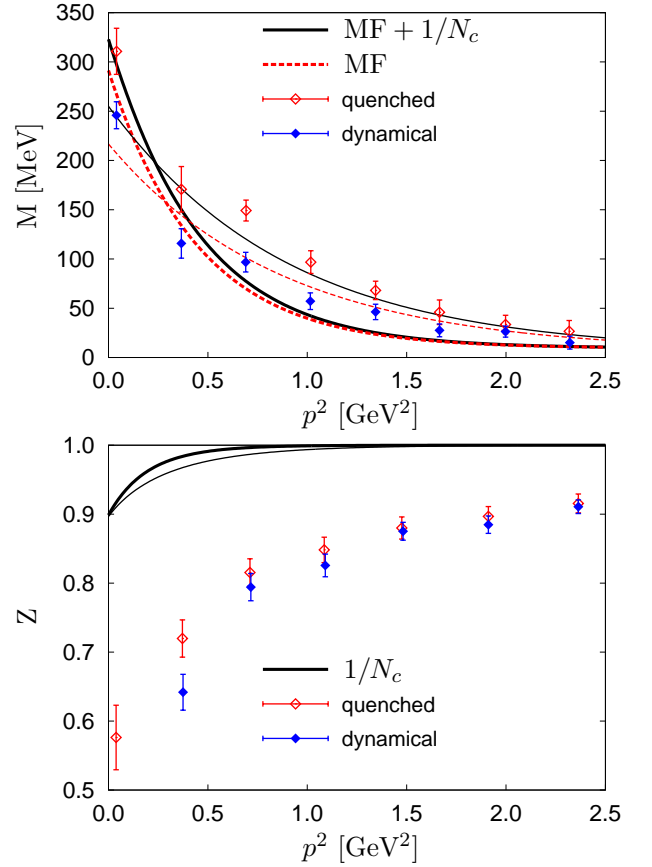


FIG. 10: (Color online) Behavior of the quark mass function (upper panel) and wave-function renormalization function (lower panel) for set No. 4 (bold lines) and set No. 2 (thin lines). The results of the full $1/N_c$ corrected approach (black solid lines) and the mean field contribution (red dashed lines) are compared with quenched (open symbols) and unquenched (full symbols) lattice data [18], extrapolated to the chiral limit.

In Fig. 10 we present a comparison of the behavior of the mass function (upper panel) and wave-function renormalization function (lower panel) in the present approach for two parameter sets (No. 2 and No. 4) with lattice data for this quantity [18] extrapolated to the chiral limit case. One can see that the gross behavior of the momentum dependence of the quark mass function as measured in lattice QCD is reflected by the nonlocal model. More in detail, the $1/N_c$ corrected result for the weaker coupling No. 2 (thin black solid line) matches the quark mass at zero-momentum, but stays above the lattice data for dynamical quarks at finite momentum transfer. The stronger coupling set No. 4 (bold black solid line), however, overestimates the quark mass function for low momenta $p^2 < 0.5 \text{ GeV}^2$ by about 25% and stays below the lattice data by about the same amount in the intermediate momentum range $0.5 \leq p^2 [\text{GeV}^2] \leq 2$.

As one can see in the lower panel of Fig. 10, the agreement of our model results for the wave-function renormalization function $Z(p)$ with the lattice data is rather

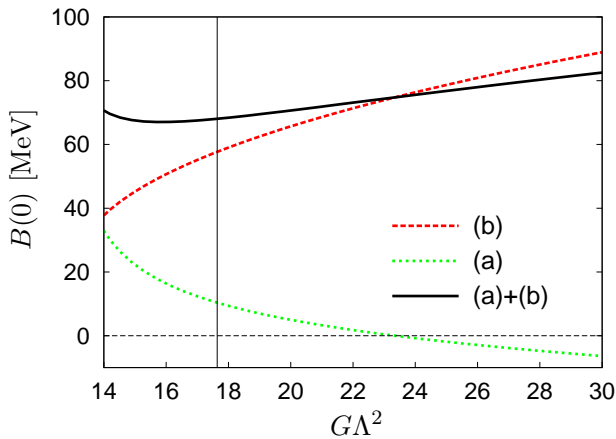


FIG. 11: (Color online) $1/N_c$ -correction to the scalar quark dressing function $B(p^2)$ at $p^2 = 0$ as a function of the dimensionless coupling $G\Lambda^2$. Also shown are the separate contributions of the diagrams (a) and (b) of Fig. 3.

poor. This is not unexpected because Dyson-Schwinger QCD calculations find a 30% reduction of $Z(p)$ at low momenta already in quenched approximation, i.e., without including meson effects [43], whereas the present model predicts $Z \equiv 1$ at mean field. A nontrivial mean-field $Z(p)$ can be obtained in the nonlocal PNJL model by adopting a suitable separable form of the interaction with vector currents with derivative coupling (rank-2 interaction), see [16, 44–46] where also a comparison with lattice QCD data can be found. In the present work which uses a separable ansatz in the scalar-pseudoscalar channel (rank-one interaction), a nontrivial wave-function renormalization arises only from the $1/N_c$ corrections. Since these contributions generally do not exceed the 10% level when compared to the mean-field, we cannot expect a quantitative description of $Z(p)$ at low momenta.

In Fig. 11 we show the $1/N_c$ correction to $B(0)$ as a function of the dimensionless coupling $G\Lambda^2$. Besides the total correction (black solid line), which is almost independent of the parameter choice, the contributions of the diagrams (a) and (b) of Fig. 3 are also indicated separately. As one can see, the dominant contribution comes from diagram (b), which is always positive.

Indeed, in Euclidean space the contribution of diagram (b) to the B -function takes the form

$$B^{N_c, (b)}(p_E^2) = f^2(p_E^2) \int \frac{d^4 q_E}{(2\pi)^4} \frac{f^2(q_+^2) m(q_+^2)}{q_+^2 + m^2(q_+^2)} \times \left[\frac{3g_\pi^2(q_E^2)}{q_E^2 + M_\pi^2} - \frac{g_\sigma^2(q_E^2)}{q_E^2 + M_\sigma^2} \right], \quad (28)$$

where we have defined $q_+ = q_E + p_E$ and

$$g_M^2(q_E^2) = \frac{q_E^2 + M_M^2}{G^{-1} - \Pi_M(q_E^2)}. \quad (29)$$

The latter is a straightforward extension of Eqs. (7) and (10) to (Euclidean) off-shell momenta. In particular, g_M^2

is strictly positive. Hence, the pion gives a positive contribution to $B^{N_c, (b)}(p_E^2)$, while the sigma contribution is negative because of the extra minus sign. Since the pions are more important, both, because of their lower mass and because of the degeneracy factor of 3, the total contribution is positive, as we have seen in Fig. 11.

Neglecting the form factors and the momentum dependencies of the quark masses and coupling constants, Eq. (28) has a natural interpretation in terms of a simple model where the quarks are coupled to pions and sigma mesons by a Yukawa interaction,

$$\mathcal{L}_{Yukawa} = -\bar{q}(x) [g_\sigma \sigma(x) + g_\pi i \gamma_5 \vec{\tau} \cdot \vec{\pi}(x)] q(x). \quad (30)$$

From this point of view, the observed enhancement of the B -function through pion loops should be the expected result. This seems to be in conflict with the Dyson-Schwinger analysis of Ref. [43] where pion loops give a negative contribution to the B -function in QCD. However, in that approach the pions have been introduced somewhat differently, namely through corrections to the quark-gluon vertex. It is interesting that this leads to the opposite sign. Understanding this different behavior deserves further study.

At first sight, our results also seem to contradict the analysis of Ref. [33] in a local NJL model, where again it was found that the B -function decreases when pion and sigma loops are included. In contrast to our present model, the $1/N_c$ -corrections have been included selfconsistently, i.e., the calculations take into account the back-reactions of the meson loops on the mean-field selfenergy. A closer inspection [47] reveals that this is the essential difference. Whereas, in complete agreement with our expectations, the meson loops themselves give a positive contribution to the B -function, their back-reaction strongly reduces the Hartree contribution, so that the total effect is a reduction of $B(0)$. In turn, this suggests that the enhancement of $B(0)$ we obtain in our model could be due to the non-selfconsistent treatment of the $1/N_c$ -corrections. On the other hand, it is a well-known problem of the fully selfconsistent scheme that the internal pions are much too heavy, so that in Ref. [33] the (positive) contribution of the pion loops is underestimated. Hence, the true sign of the correction is the result of a delicate interplay between several different processes and certainly needs further investigations.

III. FINITE TEMPERATURE

In this section we extend the model to finite temperature and then discuss the predictions for the pressure, the behavior of the quark condensate and critical temperatures.

A. Thermodynamic potential

The model can easily be extended to finite temperature using a Φ -derivable ansatz (see, e.g., Ref. [48]) supplemented by the $1/N_c$ expansion. The central quantity for the analysis is the thermodynamic potential per volume

$$\Omega = i\text{Tr} \ln(\mathbf{S}^{-1}) + i\text{Tr}(\Sigma\mathbf{S}) + \Psi(\mathbf{S}) + U(\Phi, \bar{\Phi}) - \Omega_0, \quad (31)$$

where \mathbf{S} and $\Sigma = (S^c)^{-1} - \mathbf{S}^{-1}$ are the full propagator and the quark selfenergy, respectively, and Tr denotes the trace over all degrees of freedom, internal ones and 4-momenta. At nonzero temperature, we also take into account the Polyakov-loop dynamics which no longer decouples from the quark sector. To that end a constant temporal background gauge field $\phi \equiv \langle A_4 \rangle = \langle iA_0 \rangle$ is minimally coupled to the quarks and a Polyakov loop potential $U(\Phi, \bar{\Phi})$ is added in Eq. (31). Here $\Phi = \frac{1}{N_c} \text{Tr}_c e^{i\phi/T}$ denotes the Polyakov loop expectation value and $\bar{\Phi}$ its conjugate. In order to avoid confusion with the potential of the Φ -derivable scheme (“ Φ functional”), we denote the latter as Ψ . In the exact case, Ψ contains all two-particle irreducible diagrams. Finally, we have introduced a subtractive renormalization constant Ω_0 , which is chosen such that the vacuum ($T = 0$) has vanishing pressure.

The thermodynamic equilibrium corresponds to the (global) minimum of the thermodynamic potential with respect to the full quark propagator and to the Polyakov loop, so that the following necessary conditions (gap equations) must be fulfilled

$$\frac{\partial \Omega}{\partial \mathbf{S}} = 0, \quad \frac{\partial \Omega}{\partial \Phi} = 0, \quad \frac{\partial \Omega}{\partial \bar{\Phi}} = 0. \quad (32)$$

We work in Polyakov gauge where the background gauge field is diagonal in color space, i.e., $\phi = \phi_3 \lambda_3 + \phi_8 \lambda_8$. Following [10], we require $\Phi = \bar{\Phi}$ to be real with real ϕ_3, ϕ_8 . As a consequence $\phi_8 = 0$ and we are left with one variable ϕ_3 . The second and the third equation thus reduce to $\partial \Omega / \partial \phi_3 = 0$. Moreover, the first equation implies that $\Sigma = i\delta\Psi / \delta\mathbf{S}$. Diagrammatically this means that the quark selfenergy can be obtained from Ψ by cutting one quark line at all possible places.

Approximations can be introduced by truncating Ψ at a certain order. The mean-field results, corresponding to the leading order in $1/N_c$, are obtained from the “glasses” diagram, displayed in Fig. 12. Solid lines represent dressed quark propagators. In the nonlocal model

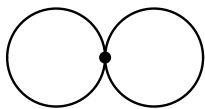


FIG. 12: Glasses diagram for the Ψ potential in the Φ -derivable scheme.

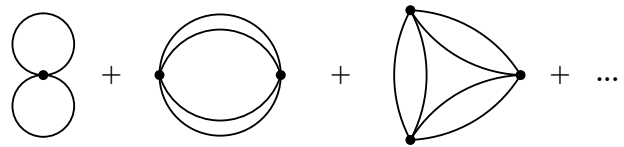


FIG. 13: Ring sum in the Ψ -potential, see Eq. (35).

the “glasses” potential takes the form

$$\Psi_{\text{glasses}} = - \sum_{M=\pi,\sigma} \frac{G}{2} [-\text{Tr}(\Gamma^M i\mathbf{S})]^2, \quad (33)$$

and the thermodynamic potential reads

$$\Omega^{\text{MF}} = \frac{m_d^2}{2G} + U(\Phi, \bar{\Phi}) - \sum_{i=0,\pm} 4 \int_{k,n} \ln [k_{n,i}^2 + M^2(k_{n,i}^2)],$$

where $k_{n,i}^2 = (\omega_n^i)^2 + \mathbf{k}^2$ and the notation $\int_{k,n} \equiv T \sum_n \int d^3k / (2\pi)^3$ has been introduced. Note that due to the coupling to the Polyakov loop the fermionic Matsubara frequencies $\omega_n = (2n+1)\pi T$ are partially shifted: $\omega_n^\pm = \omega_n \pm \phi_3$, $\omega_n^0 = \omega_n$. Apart from this shift, the modification of the quark propagator only depends on the dynamical mass m_d . Therefore at mean field the gap equations, Eq. (32), take the form

$$\frac{\partial \Omega^{\text{MF}}}{\partial m_d} = 0, \quad \frac{\partial \Omega^{\text{MF}}}{\partial \phi_3} = 0. \quad (34)$$

The next-to-leading order contribution to the Ψ -potential is given by the “ring sum”,

$$\Psi_{\text{ring}} = - \sum_{M=\pi,\sigma} \frac{d_M}{2} i\text{Tr} \ln [1 - G\Pi^M], \quad (35)$$

see Fig. 13. Here Π^M denotes the quark-antiquark polarization functions constructed with the full quark propagators and d_M is the mesonic degeneracy factor.

At this level, the problem arises that in a fully self-consistent treatment the iteration of diagrams in the gap equation leads to contributions of arbitrary orders in $1/N_c$. As a consequence, different approximation schemes can be defined. In the present paper, we use a “strict $1/N_c$ expansion”, where all contributions beyond the next-to-leading order are discarded. In the absence of the background gluon field this scheme is straightforwardly implemented by first solving the mean-field gap equation for m_d (first equation of Eq. (34)) and then evaluating the ring sum using the mean-field propagators. Thus, one gets for the thermodynamic potential

$$\Omega = \Omega^{\text{MF}} + \Omega^{\text{Nc}}, \quad (36)$$

with the $1/N_c$ correction

$$\Omega^{\text{Nc}} = \sum_{M=\pi,\sigma} \frac{d_M}{2} \int_{p,m} \ln [1 - G\Pi_M(\vec{p}, \nu_m)] \quad (37)$$

where the polarization functions $\overline{\Pi}^M$ are evaluated with mean-field propagators and summation is over bosonic Matsubara frequencies.

Including the gluon background, we suggest to treat the Polyakov-loop potential as effectively N_c independent.⁵ A strict $1/N_c$ expansion of the thermodynamic potential then corresponds to evaluate Eq. (36) for the simultaneous solutions of the gap equations

$$\frac{\partial \Omega^{\text{MF}}}{\partial m_d} = 0, \quad \frac{\partial \Omega}{\partial \phi_3} = 0. \quad (38)$$

Note that ϕ_3 is determined by minimizing the total thermodynamic potential, whereas m_d is obtained from the mean-field part only. Nevertheless, since Ω^{MF} also depends on ϕ_3 , the value of m_d is changed as well compared to the mean-field calculation, due to the modified value of ϕ_3 .

We also note that the scheme outlined above slightly differs from the scheme in our previous paper [13] where both, m_d and ϕ_3 , have been fixed at mean-field level, before inserting them into Ω^{N_c} . In the numerical calculations, however, this difference turned out to be small.

B. Finite temperature results

We now discuss our numerical results at finite temperature. In the quark sector we take the parameters of set No. 4, see Table I in Sec. II C. For the Polyakov loop potential $U(\Phi, \overline{\Phi})$ we adopt the logarithmic parametrization of Ref. [10], which has been fitted to the quenched lattice data of Ref. [51]. The only exception concerns the parameter T_0 , which corresponds to the transition temperature in pure gauge. While in Ref. [10] the empirical value $T_0 = 270$ MeV was used, it has been argued in Ref. [52] that T_0 depends on the number of active flavors and a value of 208 MeV was suggested for $N_f = 2$. Therefore our calculations will be performed using both values of T_0 .

The model predictions for the pressure are displayed in Fig. 14. The upper panel corresponds to $T_0 = 270$ MeV, the lower one to $T_0 = 208$ MeV. Together with the full result (solid lines) we show the partial contributions to the pressure from the mean-field approximation (dash-dotted lines), $P^{\text{MF}} = -\Omega^{\text{MF}}$, and from the $1/N_c$ corrections (dashed lines), $P^{N_c} = -\Omega^{N_c}$. In agreement with earlier results in PNJL-like models we find that at low

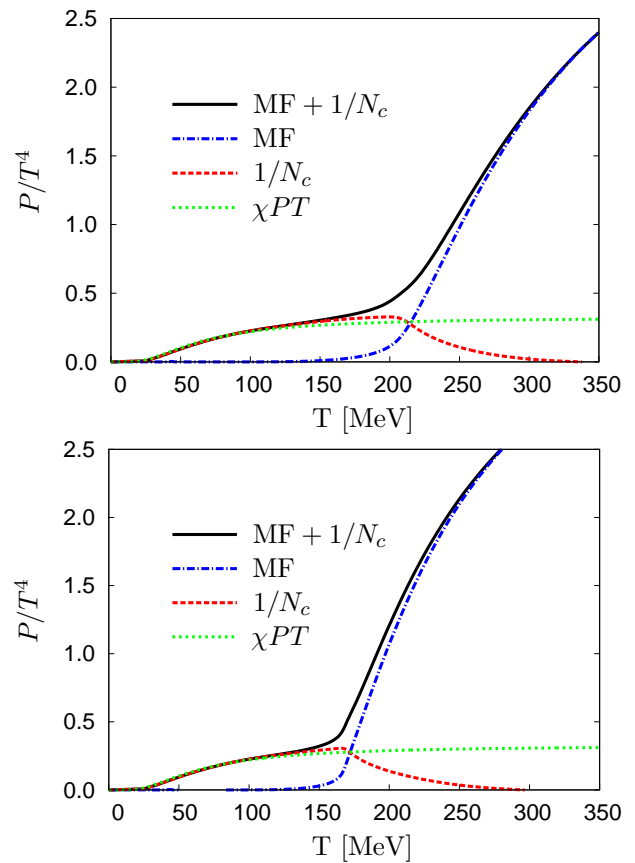


FIG. 14: (Color online) Temperature dependence of the scaled pressure P/T^4 for $T_0 = 270$ MeV (upper panel) and for $T_0 = 208$ MeV (lower panel): mean field contribution (blue dash-dotted lines), $1/N_c$ correction (red dashed lines), mean field + $1/N_c$ contributions (black solid lines). The green dotted lines correspond to the NLO chiral perturbation theory (χPT) result, Eq. (39) [53].

temperatures the mean-field contribution, corresponding to thermally excited quarks, is strongly suppressed by the Polyakov loop. In this regime the thermodynamics is governed by the ring sum, which is dominated by pionic degrees of freedom as the lightest particles in the mass spectrum. Therefore, it is instructive to compare our result with the predictions of chiral perturbation theory (χPT). χPT describes the low-energy structure of different amplitudes in terms of an expansion in powers of energies, momenta and current quark masses. The finite temperature result for the pressure is given by [53]

$$P_{\chi PT} = \frac{N_f^2 - 1}{2} \left(g_0 - \frac{1}{N_f} \frac{M_\pi^2}{2F^2} g_1^2 \right) + O(p^8),$$

$$g_0 = -2T \int \frac{d^3 p}{(2\pi)^3} \ln \left(1 - e^{-E_\pi/T} \right),$$

$$g_1 = \int \frac{d^3 p}{(2\pi)^3} \frac{1}{E_\pi (e^{E_\pi/T} - 1)}, \quad (39)$$

where F is the weak pion decay constant in the chiral limit, $E_\pi = \sqrt{\mathbf{p}^2 + M_\pi^2}$ is the pion energy, and $O(p^8)$

⁵ In principle the $U(\Phi, \overline{\Phi})$ is proportional to the number of gluons, $N_c^2 - 1$ [49, 50]. Its leading contribution to the thermodynamic potential is therefore of the order $O(N_c^2)$, while the quarks only contribute at the order $O(N_c)$ and corrections are of the order $O(N_c^0)$ for both, quarks and gluons. However, since in practice the detailed form of U is not based on a $1/N_c$ expansion, but rather a phenomenological parameterization fitted to quenched lattice data, we believe that it is more appropriate to treat it as N_c independent in the present context.

refers to the chiral counting scheme, where M_π and T count as quantities of order p . The term proportional to g_0 just represents the free relativistic pion gas pressure, while the g_1 term is caused by interactions and leads to a small reduction of the pressure.⁶ The omitted terms of order $O(p^8)$ are also due to interactions.

Recalling that the pion decay constant is of the order $\sqrt{N_c}$, we see that the g_0 and g_1^2 terms are of the order N_c^0 and $1/N_c$, respectively. Comparing this with our model, where the mean-field and ring-sum contributions to the pressure are of the order N_c and N_c^0 , respectively, we conclude that our model calculations should only be consistent with the lowest-order χPT result, i.e., with the g_0 term. Nevertheless, since the g_1^2 -term is small (it vanishes in the chiral limit), we find excellent agreement even when this term is included, see Fig. 14. Moreover, the low-temperature behavior of our model predictions is almost insensitive to the particular functional dependence of the form factor and different parameterizations. Of course, our results start to deviate from the χPT predictions when we approach the chiral phase transition. Near the critical temperature the σ meson gives an additional visible contribution whereas already for $T > 1.5 T_c$ the mesonic contributions are negligible and the quark-gluon mean-field dominates the pressure.

Comparing the upper and lower panels of Fig. 14 we observe that the lowering of T_0 also leads to a lowering of the transition temperature. However, apart from this trivial effect, the results remain qualitatively unchanged.

In Fig. 15 we show the temperature dependence of the quark condensate $\langle \bar{q}q \rangle_T$ (black solid line) and of the Polyakov loop expectation value (red dashed line) in our model beyond mean field. For comparison we also show the quark condensate in mean-field approximation (blue dash-dotted line). Again, the results for $T_0 = 270$ MeV and 208 MeV are displayed in the upper and in the lower panel, respectively. As already seen for the pressure, the $1/N_c$ corrections mainly affect the behavior of the chiral condensate below and around the critical region. In particular at low temperatures the reduction of the chiral condensate is almost entirely driven by the pion dynamics, which is missing in the mean-field approximation. In this context, it is again instructive to compare the model results with the χPT prediction. The latter is given by

$$\langle \bar{q}q \rangle_T = \langle \bar{q}q \rangle \left\{ 1 - \frac{N_f^2 - 1}{N_f} \frac{g_1}{F^2} + O(p^4) \right\}, \quad (41)$$

showing that the leading temperature effect is of the order $O(1/N_c)$. Our model results are completely consistent with this: Whereas the mean-field condensate

($O(1/N_c^0)$) stays practically constant at low T , we find very good agreement with the χPT predictions (green dotted line) after including the $1/N_c$ corrections. We should note that the chiral expansion scheme is very similar but not exactly equivalent to the $1/N_c$ counting: In χPT the leading-order correction to the chiral condensate depends on the weak pion decay constant in the chiral limit F , whereas in the $1/N_c$ expansion it depends on the weak pion decay constant for massive pions in mean-field approximation f_π^{MF} . Although formally of higher order in p or N_c , this could lead to quantitative differences, even at low temperatures. However, for the chosen parameters the difference between F and f_π^{MF} happens to be very small.

In agreement with other works [29, 33, 54], the additional reduction of the chiral condensate by the $1/N_c$ -correction terms generally also leads to a lowering of the

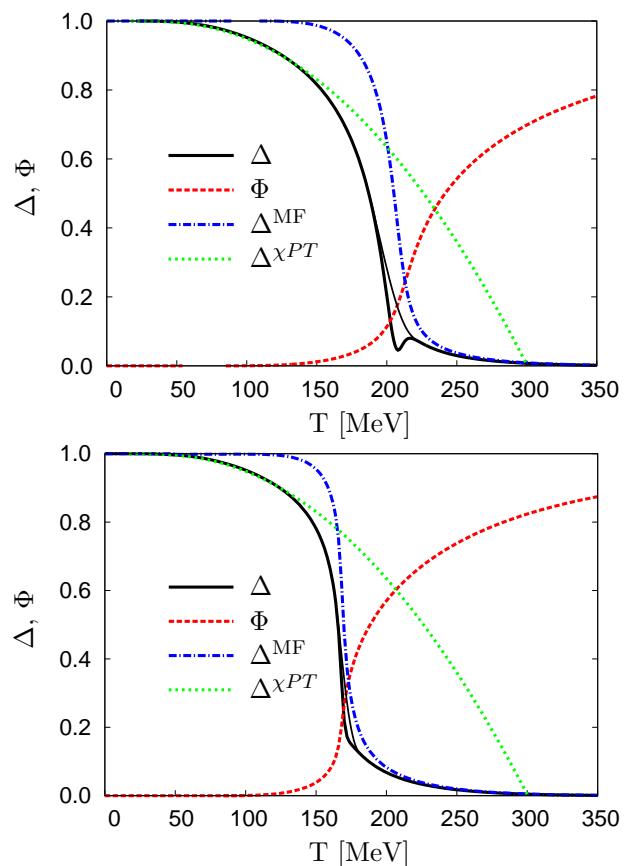


FIG. 15: (Color online) Temperature dependence of the quark condensate normalized to its vacuum value $\Delta = \langle \bar{q}q \rangle_T / \langle \bar{q}q \rangle$ (black solid lines) and the Polyakov loop (red dashed lines) in the nonlocal PNJL model beyond mean field. Furthermore shown are the mean-field result for the normalized quark condensate Δ^{MF} (blue dash-dotted lines), the lowest-order chiral perturbation theory (χPT) result (green dotted lines), and a naïve polynomial interpolation in the unstable regions of the $1/N_c$ expansion (thin black solid lines). The model calculations have been performed with $T_0 = 270$ MeV (upper panel) and with $T_0 = 208$ MeV (lower panel).

⁶ In the chiral limit g_0 and g_1 are given by

$$g_0 = \frac{\pi^2 T^4}{45}, \quad g_1 = \frac{T^2}{12}. \quad (40)$$

chiral phase-transition temperature as compared to the mean-field result. This effect is most clearly seen in the upper panel of Fig. 15, corresponding to $T_0 = 270$ MeV. Unfortunately, because of the perturbative nature of the strict $1/N_c$ -expansion scheme, our model cannot be applied to study the phase transition itself. In the figure, this is obvious from the existence of an unstable region (“wiggle”) in that region. The origin of this wiggle can be attributed to the momentum independent $1/N_c$ correction to the quark selfenergy (Fig. 3a). In the vicinity of the phase transition, this diagram is dramatically enhanced due to the restoration of chiral symmetry and the corresponding lowering of the intermediate σ -meson mass. (In fact, in the chiral limit this contribution would go to minus infinity at T_c .) As a rough estimate we define the unstable region as the regime where the relative correction to the quark condensate is larger than $1/N_c$. In the present example this corresponds to temperatures between 183 and 223 MeV. Since our results cannot be trusted in this area, we suggest to use a simple polynomial interpolation between the stable regions at lower and higher temperatures. The resulting temperature dependence is displayed in Fig. 15 by the thin black solid line.

The situation is somewhat different for $T_0 = 208$ MeV (lower panel). Although the $1/N_c$ corrections are again essential at low temperatures (in agreement with the χPT results), their effect on the chiral critical temperature is almost negligible. This is due to the fact that for this lower value of T_0 the mean-field transition takes place earlier. Related to this, the mean-field chiral condensate drops more steeply⁷. The “unstable region” where the relative correction to the quark condensate is larger than $1/N_c$ is quite narrow and the wiggle near the chiral phase transition, which we found for $T_0 = 270$ MeV, is not present for $T_0 = 208$ MeV.

A systematic overview about the T_0 -dependence of the pseudocritical temperatures for deconfinement (red dashed line) and chiral restoration (solid black line) is given in Fig. 16. As definitions of these temperatures we have chosen the maxima of the temperature derivatives of the corresponding order parameter, i.e., Polyakov-loop expectation value and chiral condensate, respectively. In the unstable regime (indicated by the shaded area) the latter was obtained from the polynomial interpolation. The mean-field result for the chiral-restoration temperature is also shown (blue dashed-dotted line).

In this figure, we can roughly distinguish three regimes: At large values of T_0 already the mean-field T_c is lower than T_d , and T_c is even lowered further by including $1/N_c$ corrections. Then, in some intermediate regime, T_d and T_c agree at mean field but there is still a visible reduction of the latter by the $1/N_c$ corrections. Finally, for $T_0 \lesssim$

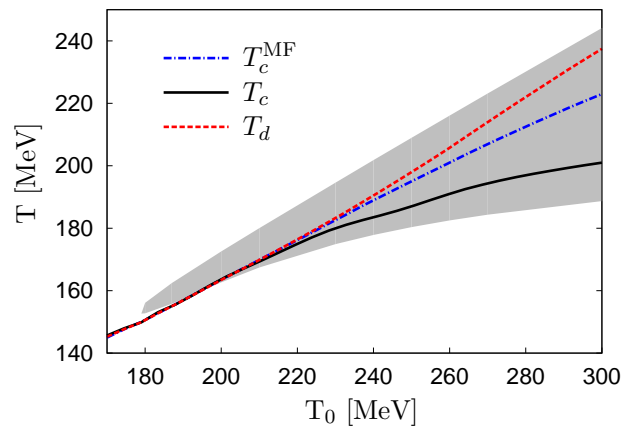


FIG. 16: (Color online) Critical temperatures versus the parameter T_0 of the Polyakov-loop potential: deconfinement (red dashed line), chiral restoration in mean-field (blue dash-dotted line), chiral restoration with mesonic fluctuations (black solid line). The region with $|\langle \bar{q}q \rangle_T^{N_c} / \langle \bar{q}q \rangle_T^{MF}| > 1/N_c$ is indicated by the shaded area.

220 MeV all three lines practically coincide.⁸

To understand this behavior we should recall that without coupling between quark and Polyakov-loop sector, T_0 corresponds to the (first-order) deconfinement-transition temperature, while the chiral cross-over in the nonlocal model takes place at a very low temperature, $T_c^{MF} = 116$ MeV. From this point of view it is quite remarkable that even for $T_0 = 270$ MeV the coupling reduces the difference between T_c^{MF} and T_d to less than 10 MeV. Nevertheless, the synchronization obviously works better when T_0 is reduced and eventually becomes perfect for $T_0 \lesssim 220$ MeV. Related to this, the transitions get sharper with decreasing T_0 and the relative effect of the $1/N_c$ corrections on T_c is reduced as well, as we have seen above.

At this point we should note that the Polyakov-loop dynamics and, hence, the deconfinement transition are quite insensitive to the $1/N_c$ corrections. This is most likely an artifact of the model where the Polyakov-loop is affected by the meson back-coupling only in a very indirect way (see the discussion after Eq. (38)). In principle, mesonic fluctuations should also directly influence the Polyakov-loop potential. However, it is not clear how to include this in PNJL-like models, where the potential is obtained from a phenomenological fit of quenched lattice data where even the effects of dynamical quarks are neglected (except for changes in T_0). In this context it

⁷ For $T_0 \lesssim 150$ MeV, the phase transition even becomes first order. A similar observation was recently made in Ref. [16].

⁸ According to Table I the $1/N_c$ corrections can even enhance the value of T_c by 1 or 2 MeV at $T_0 = 208$ MeV. However, since cross-over temperatures are not defined in a unique way, and even rely on the polynomial interpolations in the present case, this should not be over-interpreted. If we had defined T_c as the temperature where the condensate reaches half of its vacuum value, the $1/N_c$ corrections would always lead to a reduction of T_c .

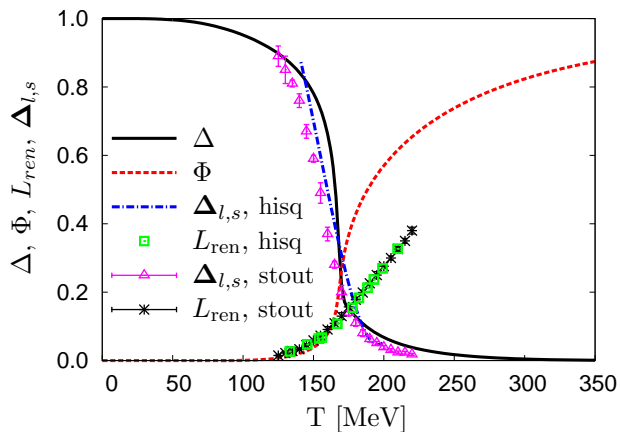


FIG. 17: (Color online) Temperature dependence of the quark condensate normalized to its vacuum value $\Delta = \langle \bar{q}q \rangle_T / \langle \bar{q}q \rangle$ (black solid line) and the Polyakov loop (red dashed line) in the nonlocal PNJL model with $T_0 = 208$ MeV beyond mean field in comparison with lattice QCD data for the subtracted quark condensate $\Delta_{l,s}$ and for the renormalized Polyakov loop L_{ren} . Lattice points are taken from [19] (hisq action – HotQCD collaboration) and [20] (stout action – Wuppertal-Budapest collaboration).

would certainly be interesting to compare the behavior of the Polyakov loop with the so-called dressed Polyakov loop, related to the dual quark condensate [55, 56]. The latter can be calculated within PNJL-like [57] (and even NJL models [58]) and it should be possible to study $1/N_c$ corrections as well. However, this is beyond the scope of the present paper.

In Fig. 17 we present the comparison of our prediction for the temperature dependence of quark condensate and Polyakov loop with recent lattice data [19, 20]. The model calculations are performed with $T_0 = 208$ MeV, which leads to the more realistic transition temperatures. One should mention that the lattice calculations [19, 20] are performed for the case of two light quarks and one strange, $N_f = 2 + 1$. For the investigation of the quark condensate they use a combination of nonstrange(l) and strange(s) quark condensates, called subtracted quark condensate,

$$\Delta_{l,s} = \frac{\langle \bar{q}q \rangle_T^l - \frac{m_c^l}{m_c^s} \langle \bar{q}q \rangle_T^s}{\langle \bar{q}q \rangle^l - \frac{m_c^l}{m_c^s} \langle \bar{q}q \rangle^s}. \quad (42)$$

In the present paper we consider a model with only two light active flavors. Nevertheless, it makes sense to perform the comparison of our calculation for the temperature dependence of the quark condensate normalized to its vacuum value $\Delta = \langle \bar{q}q \rangle_T / \langle \bar{q}q \rangle$ with the lattice calculations of the subtracted quark condensate. The reason is that the nonperturbative part of the quark condensate in Eq. (6) is finite and the strange quark contribution in Eq. (42) is suppressed in the nonlocal model by two factors: (i) the ratio of the nonperturbative part of the strange quark condensate to that of the nonstrange one

is 0.8 and the ratio of the nonstrange current quark mass to the strange one is about 1/20. On the other hand the main role for low temperature changes of the quark condensate is played by pions - an effect which is correctly accounted for in our model.

Indeed, we find that $\Delta_{l,s}$ is rather well reproduced by our model calculations for Δ . For the Polyakov loop, on the other hand, we find good agreement only at the onset, whereas around the deconfinement temperature, $T \approx 170$ MeV, the model prediction rises much steeper than the lattice data. This seems to indicate that there is missing physics, which is not captured by just rescaling the temperature T_0 of the pure-gluon potential.

IV. SUMMARY

In the present work, we have extended the nonlocal chiral quark model, coupled to the Polyakov loop, beyond the mean field approximation using a strict $1/N_c$ expansion scheme. In vacuum, it is found that $1/N_c$ corrections lead to an increase of the quark condensate, which is opposite to results obtained in the NJL model with local interactions. However, the result of the local model is strongly dependent on the mesonic cut-off and for large values of the cut-off ($\Lambda_M > 1.5$ GeV) the sign of the correction is positive in both models.

The parameters of the nonlocal model have been refitted in vacuum to reproduce the physical values of the pion mass and the weak pion decay constant after including the $1/N_c$ corrections. In agreement with general expectations, we find that the mean field gives the dominant contribution to the pion properties, while the maximal size of the $1/N_c$ corrections to the pion mass and weak pion decay constant amounts to 15 and 20 MeV, respectively.

At finite temperature, the $1/N_c$ corrections lead to a reduction of the chiral condensate when compared to the mean-field result. Typically, this also leads to a reduction of the chiral phase transition temperature. However, for lower values of the parameter T_0 in the Polyakov-loop potential, the mean-field transition becomes steeper and, thus, the effect of the $1/N_c$ corrections on T_c becomes smaller. Eventually, for $T_0 \lesssim 220$ MeV, T_c remains practically unaffected by the $1/N_c$ corrections. For low temperatures, $T \leq 100$ MeV, our result for the quark condensate practically coincides with that of χPT whereas the high-temperature region is well controlled by the mean-field approximation.

In the chiral limit our expansion scheme, which treats the $1/N_c$ corrections perturbatively, breaks down in the vicinity of the chiral phase transition. For the real case of nonzero current quark masses a similar situation takes place for large values of the T_0 parameters of the Polyakov loop potential (e.g., $T_0 = 270$ MeV in the pure gluodynamics case). Alternatively, one could include the mesonic fluctuations non-perturbatively, as done in Ref. [33] for the local NJL model. In that anal-

ysis it was found as well that mesonic fluctuations lead to a decrease of the critical temperature, but the unstable region around the phase transition is absent. On the other hand, the low-temperature behavior of χPT is not reproduced in this scheme. It seems plausible that the inclusion of higher-order corrections could make both expansion schemes converge to one another, i.e., in the strict $1/N_c$ expansion the unstable region will be reduced (except close to a real phase transition) while in the self-consistent scheme the low-temperature behavior will get closer to the χPT predictions.

Concerning the pressure, we confirm our previous result [13] that the pionic contribution dominates in the low temperature region. In this regime, the pressure is quite insensitive to the details of the interaction and agrees almost exactly with that of an ideal pion gas. At temperatures $T > T_c$, on the other hand, the mesonic contributions die out at $T \sim 1.5 T_c$.

As a next step, we plan to study nonzero chemical potentials, which may require a nontrivial extrapolation of the Polyakov-loop potential into this regime [52]. The treatment of the entire $T-\mu$ plane of the QCD phase diagram finally requires the inclusion of baryonic degrees of freedom as well.

Acknowledgments

We thank C. Fischer, D. Müller, J. Wambach, and R. Williams for critical remarks and illuminating discussions. A.E.R. is grateful for the hospitality extended to him during visits at the TU Darmstadt and at the University of Wrocław. We acknowledge support by the Heisenberg-Landau programme (M.B., A.E.R., M.K.V.), by EMMI (A.E.R.), by the Russian Foundation for Basic Research under contracts No. 09-02-00749 (A.E.R.), No. 08-02-01003-a and No. 11-02-01538-a (D.B.), a grant of the Russian President (A.E.R.), and by the Polish Ministry of Science and Higher Education under the CompStar-POL grant and grant No. NN 202 231837 (D.B.), as well as by CompStar, a Research Networking Programme of the European Science Foundation.

Appendix A: $1/N_c$ corrections to the pion propagator and the weak decay constant

The $1/N_c$ corrections to the meson propagator consist of the diagrams shown in Fig. 18. For convenience we divide them into three types. For the pion the corresponding expressions take the form

$$\begin{aligned} \Pi_{\pi,1a+2a}^{N_c}(p^2) &= i \int \frac{d^4k}{(2\pi)^4} \times \\ &\times \text{Tr} \left[\Gamma_{k_+,k_-}^\pi S_{k_-} \Sigma_{k_-}^{N_c} S_{k_-} \Gamma_{k_-,k_+}^\pi S_{k_+} \right] \\ \Pi_{\pi,1b+2b}^{N_c}(p^2) &= i \int \frac{d^4k}{(2\pi)^4} \times \\ &\times \text{Tr} \left[\Gamma_{k_+,k_-}^\pi S_{k_-} \Gamma_{k_-,k_+}^\pi S_{k_+} \Sigma_{k_+}^{N_c} S_{k_+} \right] \end{aligned}$$

$$\begin{aligned} \Pi_{\pi,2c}^{N_c}(p^2) &= \sum_{M=\sigma,\pi} \int \frac{d^4k}{(2\pi)^4} \int \frac{d^4l}{(2\pi)^4} \times \\ &\times \text{Tr} \left[\Gamma_{k_+,k_-}^\pi S_{k_-} \Gamma_{k_-,l_-}^M S_{l_-} \Gamma_{l_-,l_+}^\pi S_{l_+} \Gamma_{l_+,k_+}^M S_{k_+} \right] D_{k_-}^M \\ \Pi_{\pi,3a}^{N_c}(p^2) &= 4 \times i \int \frac{d^4k}{(2\pi)^4} \Gamma_{k_+,k_-}^{\pi\pi\sigma} D_{k_-}^\pi \Gamma_{k_-,k_+}^{\pi\sigma\pi} D_{k_+}^\sigma, \end{aligned} \quad (\text{A1})$$

where the factor 4 in $\Pi_{\pi,3a}^{N_c}(p^2)$ is the degeneracy factor.

The calculation of the weak pion decay constant is more complicated. Namely, part of the diagrams can be obtained from the pion propagator times $-ig_\pi^{\text{MF}}$ and substitution of the outgoing pion vertex by the vertex with an external current. Furthermore, there are additional nonlocal diagrams, shown in Fig. 19.

The additional $1/N_c$ corrections of type 1 are

$$\begin{aligned} f_{\pi,1c}^{N_c}(p^2) &= g_\pi^{\text{MF}} C \int \frac{d^4k}{(2\pi)^4} f^2(k) \text{Tr} \left[\Gamma_{k,k}^{5\pi,L} S_k \Gamma_{k,k}^\sigma S_k \right] \\ f_{\pi,1d}^{N_c}(p^2) &= g_\pi^{\text{MF}} C \int \frac{d^4k}{(2\pi)^4} \text{Tr} \left[\Gamma_{k_+,k_-}^\pi S_{k_-} \Gamma_{k_-,k_+}^{5\sigma,L} S_{k_+} \right], \end{aligned}$$

the $1/N_c$ corrections of type 2 take the form

$$\begin{aligned} f_{\pi,2d}^{N_c}(p^2) &= g_\pi^{\text{MF}} \int \frac{d^4k}{(2\pi)^4} \int \frac{d^4l}{(2\pi)^4} \times \\ &\times \text{Tr} \left[\Gamma_{k,k}^{5\pi,L} S_k \Gamma_{k,l}^M S_l \Gamma_{l,k}^M S_k \right] D_{k-l}^M \\ f_{\pi,2e}^{N_c}(p^2) &= g_\pi^{\text{MF}} \int \frac{d^4k}{(2\pi)^4} \int \frac{d^4l}{(2\pi)^4} \times \\ &\times \text{Tr} \left[\Gamma_{k_+,k_-}^\pi S_{k_-} \Gamma_{k_-,l_-}^M S_{l_-} \Gamma_{l_-,k_+}^{5M,L} S_{k_+} \right] D_{k-l}^M \\ f_{\pi,2f}^{N_c}(p^2) &= g_\pi^{\text{MF}} \int \frac{d^4k}{(2\pi)^4} \int \frac{d^4l}{(2\pi)^4} \times \\ &\times \text{Tr} \left[\Gamma_{k_+,k_-}^\pi S_{k_-} \Gamma_{k_-,l_+}^{5M,L} S_{l_+} \Gamma_{l_+,k_+}^M S_{k_+} \right] D_{k-l}^M \end{aligned}$$

and should be summed over $M = \pi, \sigma$.

The additional type-3 corrections are

$$f_{\pi,3b+3c}^{N_c}(p^2) = 2 \times g_\pi^{\text{MF}} i \int \frac{d^4k}{(2\pi)^4} \Gamma_{k_+,k_-}^{\pi\pi\sigma} D_{k_-}^\pi \Gamma_{k_-,k_+}^{5\sigma\pi,L} D_{k_+}^\sigma,$$

where the effective vertex $\Gamma_{q_1,q_2}^{5\sigma\pi,L}$ is

$$\begin{aligned} \Gamma_{q_1,q_2}^{5\beta\gamma,L} &= - \int \frac{d^4l}{(2\pi)^4} \text{Tr} \left[\Gamma_{l+q_1,l+q_2}^{5\gamma,L} S_{l+q_2} \Gamma_{l+q_2,l}^\beta S_l + \right. \\ &\left. + \Gamma_{l+q_1,l+q_2}^{5\beta,L} S_l \Gamma_{l,l+q_1}^\gamma S_{l+q_1} \right]. \end{aligned} \quad (\text{A2})$$

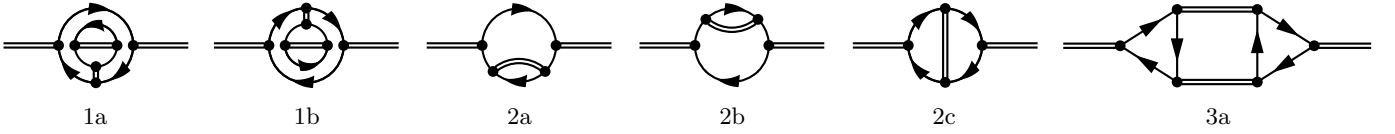


FIG. 18: Diagrams for the calculation of $1/N_c$ corrections to the meson propagator.

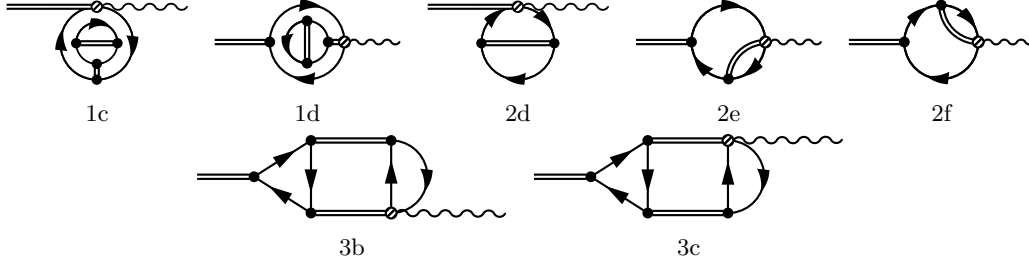


FIG. 19: Additional nonlocal diagrams for the calculation of $1/N_c$ corrections to the weak pion decay.

-
- [1] Y. Nambu and G. Jona-Lasinio, Phys. Rev. **122**, 345 (1961); Phys. Rev. **124**, 246 (1961).
- [2] M. K. Volkov, Annals Phys. **157**, 282 (1984); Sov. J. Part. Nucl. **17**, 186 (1986).
- [3] S. Klimt, M. Lutz, U. Vogl and W. Weise, Nucl. Phys. A **516**, 429 (1990); Nucl. Phys. A **516**, 469 (1990).
- [4] S. P. Klevansky, Rev. Mod. Phys. **64**, 649 (1992).
- [5] T. Hatsuda and T. Kunihiro, Phys. Rept. **247**, 221 (1994).
- [6] P. N. Meisinger and M. C. Ogilvie, Phys. Lett. B **379**, 163 (1996).
- [7] K. Fukushima, Phys. Lett. B **591**, 277 (2004).
- [8] E. Megias, E. Ruiz Arriola and L. L. Salcedo, Phys. Rev. D **74**, 065005 (2006).
- [9] C. Ratti, M. A. Thaler, and W. Weise, Phys. Rev. D **73**, 014019 (2006).
- [10] S. Rößner, C. Ratti, and W. Weise, Phys. Rev. D **75**, 034007 (2007).
- [11] C. Sasaki, B. Friman and K. Redlich, Phys. Rev. D **75**, 074013 (2007).
- [12] H. Hansen, W. M. Alberico, A. Beraudo, A. Molinari, M. Nardi, and C. Ratti, Phys. Rev. D **75**, 065004 (2007).
- [13] D. Blaschke, M. Buballa, A. E. Radzhabov and M. K. Volkov, Phys. Atom. Nucl. **71**, 1981 (2008).
- [14] G. A. Contrera, D. Gomez Dumm and N. N. Scoccola, Phys. Lett. B **661**, 113 (2008).
- [15] T. Hell, S. Rößner, M. Cristoforetti and W. Weise, Phys. Rev. D **81**, 074034 (2010).
- [16] D. Horvatic, D. Blaschke, D. Klabucar and O. Kaczmarek, arXiv:1012.2113 [hep-ph].
- [17] K. I. Kondo, Phys. Rev. D **82**, 065024 (2010).
- [18] W. Kamleh, P. O. Bowman, D. B. Leinweber, A. G. Williams, J. Zhang, Phys. Rev. **D76**, 094501 (2007).
- [19] A. Bazavov and P. Petreczky [HotQCD Collaboration], arXiv:1009.4914 [hep-lat].
- [20] S. Borsanyi, Z. Fodor, C. Hoelbling, S. D. Katz, S. Krieg, C. Ratti and K. K. Szabo [Wuppertal-Budapest Collaboration], JHEP **1009**, 073 (2010).
- [21] J. Braun, L. M. Haas, F. Marhauser and J. M. Pawłowski, Phys. Rev. Lett. **106**, 022002 (2011).
- [22] C. Amsler *et al.* [Particle Data Group], Phys. Lett. B **667**, 1 (2008).
- [23] E. Quack and S. P. Klevansky, Phys. Rev. C **49**, 3283 (1994).
- [24] D. Ebert, M. Nagy, and M. K. Volkov, Phys. Atom. Nucl. **59**, 140 (1996).
- [25] E. N. Nikolov, W. Broniowski, C. V. Christov, G. Ripka, and K. Goeke, Nucl. Phys. A **608**, 411 (1996).
- [26] V. Dmitrasinovic, H. J. Schulze, R. Tegen and R. H. Lemmer, Annals Phys. **238**, 332 (1995).
- [27] D. Blaschke, Yu. L. Kalinovsky, G. Röpke, S. M. Schmidt and M. K. Volkov, Phys. Rev. C **53**, 2394 (1996).
- [28] M. Oertel, M. Buballa and J. Wambach, Phys. Lett. B **477**, 77 (2000).
- [29] M. Oertel, M. Buballa and J. Wambach, Phys. Atom. Nucl. **64**, 698 (2001).
- [30] R. S. Plant and M. C. Birse, Nucl. Phys. A **703**, 717 (2002).
- [31] R. G. Jafarov and V. E. Rochev, Central Eur. J. Phys. **2**, 367 (2004).
- [32] K. Goeke, M. M. Musakhanov and M. Siddikov, Phys. Rev. D **76**, 076007 (2007).
- [33] D. Müller, M. Buballa and J. Wambach, Phys. Rev. D **81**, 094022 (2010).
- [34] G. 't Hooft, Nucl. Phys. B **72**, 461 (1974).
- [35] D. Gomez Dumm, A. G. Grunfeld, N. N. Scoccola, Phys. Rev. **D74**, 054026 (2006).
- [36] J. Terning, Phys. Rev. D **44**, 887 (1991).
- [37] R. D. Bowler and M. C. Birse, Nucl. Phys. A **582**, 655 (1995).
- [38] R. S. Plant and M. C. Birse, Nucl. Phys. A **628**, 607 (1998).
- [39] A. E. Dorokhov and W. Broniowski, Eur. Phys. J. C **32**, 79 (2003).
- [40] A. Scarpettini, D. Gomez Dumm and N. N. Scoccola, Phys. Rev. D **69**, 114018 (2004).
- [41] M. Bhagwat, M. A. Pichowsky and P. C. Tandy, Phys.

- Rev. D **67**, 054019 (2003).
- [42] H. Grigorian, Phys. Part. Nucl. Lett. **4**, 223 (2007).
- [43] C. S. Fischer, D. Nickel, J. Wambach, Phys. Rev. **D76**, 094009 (2007).
- [44] S. Noguera and N. N. Scoccola, Phys. Rev. D **78**, 114002 (2008).
- [45] G. A. Contrera, M. Orsaria, and N. N. Scoccola, Phys. Rev. D **82**, 054026 (2010).
- [46] T. Hell, K. Kashiwa, and W. Weise, arXiv:1104.0572 [hep-ph].
- [47] D. Müller, private communication.
- [48] G. Ripka, "Quarks bound by chiral fields: The quark-structure of the vacuum and of light mesons and baryons," *Oxford, UK: Clarendon Pr. (1997)*.
- [49] L. McLerran, K. Redlich and C. Sasaki, Nucl. Phys. A **824**, 86 (2009).
- [50] R. D. Pisarski, Phys. Rev. D **62**, 111501 (2000).
- [51] O. Kaczmarek, F. Karsch, P. Petreczky and F. Zantow, Phys. Lett. B **543**, 41 (2002).
- [52] B.-J. Schaefer, J. M. Pawłowski and J. Wambach, Phys. Rev. D **76**, 074023 (2007).
- [53] J. Gasser and H. Leutwyler, Phys. Lett. B **184**, 83 (1987).
- [54] J. Braun, Phys. Rev. D **81**, 016008 (2010).
- [55] E. Bilgici, F. Bruckmann, C. Gatttringer and C. Hagen, Phys. Rev. D **77**, 094007 (2008).
- [56] C. S. Fischer, Phys. Rev. Lett. **103**, 052003 (2009).
- [57] K. Kashiwa, H. Kouno and M. Yahiro, Phys. Rev. D **80**, 117901 (2009).
- [58] T. K. Mukherjee, H. Chen and M. Huang, Phys. Rev. D **82**, 034015 (2010).